# A two-component jet model for the tidal disruption event Swift J164449.3+573451

*Dangbo Liu*[1,2], *Asaf Pe'er*[1,3], *Abraham Loeb*[1]

[1]*Institute for Theory and Computation, Harvard-Smithsonian Center for Astrophysics, 60 Garden Street, Cambridge, MA 02138, USA*

[2]*Institute of Nuclear, Particle, Astronomy and Cosmology, Department of Physics and Shanghai Key Lab for Particle Physics and Cosmology, Shanghai Jiao Tong University, 800 Dongchuan Road, Shanghai, 200240, China*

[3]*Physics Department, University College Cork, Cork, Ireland*

## ABSTRACT

We analyze both the early and late time radio and X-ray data of the tidal disruption event Swift J1644+57. The data at early times ($\lesssim 5$ days) necessitates separation of the radio and X-ray emission regions, either spatially or in velocity space. This leads us to suggest a two component jet model, in which the inner jet is initially relativistic with Lorentz factor $\Gamma \approx 15$, while the outer jet is trans-relativistic, with $\Gamma \lesssim 1.2$. This model enables a self-consistent interpretation of the late time radio data, both in terms of peak frequency and flux. We solve the dynamics, radiative cooling and expected radiation from both jet components. We show that while during the first month synchrotron emission from the outer jet dominates the radio emission, at later times radiation from ambient gas collected by the inner jet dominates. This provides a natural explanation to the observed re-brightening, without the need for late time inner engine activity. After 100 days, the radio emission peak is in the optically thick regime, leading to a decay of both the flux and peak frequency at later times. Our model's predictions for the evolution of radio emission in jetted tidal disruption events can be tested by future observations.

*Subject headings:* black hole physics — galaxies: jets — galaxies: nuclei — — radiation mechanisms:non-thermal

## 1. Introduction

A stray star, when passing near a massive black hole (MBH) can be torn apart by gravitational forces, leading to a tidal disruption event (TDE). Such an event would be

observed as bright emission from a previously dormant MBH, as it is being fed by temporary mass accretion established after the tidal disruption of a passing star (Hills 1975; Rees 1988; Evans & Kochanek 1989). On 25 March 2011, an unusual transient source Swift J164449.3+573451 (hereafter Sw J1644+57) was reported, potentially representing such an event (Burrows et al. 2011; Levan et al. 2011). This event was found to be in positional coincidence ($\lesssim 0.2$ kpc) with a previously dormant host galaxy nucleus, at redshift $z = 0.354$ (Levan et al. 2011; Fruchter et al. 2011; Berger et al. 2011).

The rapid variability seen in the X-rays, of $\sim 78$ s (Burrows et al. 2011; Bloom et al. 2011), implies a compact source size $\lesssim 0.15$ AU, which is a few times the Schwarzschild radius of $10^6 M_\odot$ MBH (see also Miller & Gültekin 2011). When combined with the very high $\gamma$-ray and X-ray luminosity, $\approx 10^{47}\,\mathrm{erg\,s^{-1}}$ (Burrows et al. 2011; Bloom et al. 2011), which is 2 - 3 orders of magnitude above the Eddington limit of such a MBH, it was concluded that the X-ray emission must originate from a relativistic jet of Lorentz factor $\Gamma \gtrsim 10$ (Bloom et al. 2011) (see, however, Krolik & Piran 2011; Ouyed et al. 2011; Quataert & Kasen 2012; Socrates 2012, for alternative models).

While early works that investigated the expected signal (optical/UV emission) from such an event were focused on the signal from the accreting material of the stellar debris (Rees 1988; Loeb & Ulmer 1997; Ulmer 1999; Bogdanović et al. 2004; Guillochon et al. 2009; Strubbe & Quataert 2009), recently, the observational signature from a newly formed jet was considered (Giannios & Metzger 2011; van Velzen et al. 2011; Wang & Cheng 2012; Metzger et al. 2012; De Colle et al. 2012; Stone & Loeb 2012). The basic mechanism suggested in these works is similar to the mechanism that is thought to operate in gamma-ray bursts (GRBs), namely energy dissipation by either internal shock waves (Rees & Meszaros 1994; Paczynski & Xu 1994) or by an external (forward) shock wave, accompanied at early stages by a reverse shock wave (Rees & Meszaros 1992; Meszaros & Rees 1993; Piran et al. 1993; Sari & Piran 1995). These shock waves, in turn, are believed to accelerate particles and generate strong magnetic fields, thereby producing synchrotron radiation, accompanied by synchrotron self Compton (SSC) emission at high energies.

Indeed, shortly after its discovery, an extensive radio campaign showed that the X-ray emission is accompanied by bright radio emission (Zauderer et al. 2011), which was interpreted as synchrotron emission from the jetted material, thereby supporting this hypothesis. However, a careful analysis revealed that the radio emitting material propagates at a more modest Lorentz factor, $\Gamma \gtrsim 1$ (Zauderer et al. 2011), and therefore the X-ray and radio emission cannot have similar origin. This had led to the suggestion that the X-rays may originate from internal dissipation (Wang & Cheng 2012), while the radio may originate from the forward shock that propagates into the surrounding material (Metzger et al. 2012;

Cao & Wang 2012).

Late time radio monitoring, extending up to $\approx 216$ days (Berger et al. 2012), revealed an unexpected behavior: after about $\sim 30$ days (observed time), the radio emission showed re-brightening, which lasted up to $\sim 100$ days, after which the radio flux decayed. This re-brightening was not accompanied by re-brightening in the X-ray flux, and is not expected in the context of the forward shock models. This led Berger et al. (2012) to conclude that the radio re-brightening resulted from late time energy injection. Thus, a comprehensive model that considers the temporal as well as combined radio and X-ray spectral data is still lacking.

Any such model must take into account the fact that the emitting material is mildly relativistic at most. First, the radio emitting material propagates at Lorentz factor $\Gamma \gtrsim 1$. Second, while the X-ray emitting material propagates at initial Lorentz factor $\Gamma \simeq 10 - 20$, its velocity becomes trans-relativistic on the relevant time scale of tens of days, as surrounding material is collected. The dynamics of such trans-relativistic propagation was recently considered by Pe'er (2012).

Here, we propose a new model that considers simultaneously the emission of both the radio and the X-rays, their spectrum as well as temporal evolution. We re-derive the constraints set by both radio and X-ray observations, and confirm that indeed at early times (first few days) these must have a separate origin. We calculate the dynamics of the X-ray emitting plasma as it collects material from the surrounding and decelerates. We show that after $\sim 30$ days (observed time), synchrotron emission from this plasma peaks at radio frequencies, thereby providing a natural explanation to the re-brightening seen at radio frequencies at these times, without the need for late time internal engine activity. Moreover, we show that the decay of the radio flux after $\sim 100$ days is naturally explained by synchrotron self absorption. At this stage, the flow is in the trans-relativistic regime ($\Gamma - 1 \simeq 1$).

This paper is organized as follows. In §2, we carefully revise the observed data of both the radio and X-ray emission at early times (up to five days). While our treatment is more general than previous works, we confirm earlier conclusions that indeed the radio and X-ray emission must have separate origins. In §3 we consider the temporal evolution of the X-ray emitting material as it slows and cools, and show that it can be the source of the re-brightening at radio frequencies seen after $\sim 30$ days. We further consider radiative cooling in §3.2. We show that the very late ($\gtrsim 100$ days) decay of the radio flux is naturally attributed to emission in the optically thick regime: as the electrons cool, eventually the peak of the synchrotron becomes obscured. We compare our model to the late time radio data of Sw J1644+57 in §4, before summarizing our main results in §5.

## 2. Early time radio and X-ray emission and its interpretation

Sw J1644+57 is a long-lived (duration $\gtrsim$ months) X-ray outburst source, accompanied by bright radio emission, interpreted as synchrotron radiation. During the first few days of observations, the isotropic X-ray luminosity ranged from $\sim 3\times10^{45}\,{\rm erg\,s^{-1}}$ to a peak as high as $\sim 3\times10^{48}\,{\rm erg\,s^{-1}}$ (Burrows et al. 2011) with average X-ray luminosity $\approx few\times10^{47}\,{\rm erg\,s^{-1}}$. The X-ray emission peaked at frequency $\sim 2\times10^{18}$ Hz, with estimated uncertainty up to two orders of magnitude above this value (Zauderer et al. 2011). During the first few days, the X-ray lightcurve was complex and highly variable, with variability time scale as short as $\sim 100$ s (Burrows et al. 2011; Levan et al. 2011).

This source triggered a radio campaign, that began a few days after its initial discovery. Radio observations showed that the peak frequency occurs at $\sim 8\times10^{11}\eta$ Hz with uncertainty $1\leq\eta\leq10$, and peak luminosity $\nu L_\nu\gtrsim10^{43.5}\,{\rm erg\,s^{-1}}$ during the first few days. The spectral energy distribution (SED) at the radio band ($<345$ GHz) at $\Delta t^{\rm ob}\approx5$ days is well described by a power law, $F_\nu\propto\nu^{1.3}$ up to $F_\nu(|_{\nu=345{\rm GHz}})\approx35$ mJy. The steep power law index requires self-absorbed synchrotron emission, with self absorption frequency $\nu_a\gtrsim10^{11}$ Hz (Zauderer et al. 2011; Berger et al. 2012). Within two weeks, the X-rays maintained a more steady level, albeit with episodic brightening and fading spanning more than an order of magnitude in flux, while the low frequency (radio) emission decreased markedly (Levan et al. 2011; Zauderer et al. 2011).

### 2.1. Interpretation of early radio emission

The radio emission observed from Swift J1644+57 is assumed to have synchrotron origin. The synchrotron emitting plasma can be described by five free parameters: the source size $R$, bulk Lorentz factor $\Gamma$, total number of radiating electrons $N_{\rm e}$, magnetic field strength $B$, and the characteristic electron Lorentz factor (as is measured in the plasma frame), $\gamma_e$. Calculations of the values of these parameters appear in Zauderer et al. (2011). Here, we generalize the treatment in Zauderer et al. (2011) by removing the equipartition assumption used in that work.

Existing data provides the following four constraints. The observed characteristic frequency and total luminosity of synchrotron emission, $\nu_m^{\rm ob}$ and $\nu L_\nu$ are given by (Rybicki & Lightman 1979)

$$\begin{aligned}\nu_m^{\rm ob} &= \tfrac{3}{4\pi}\tfrac{q_eB}{m_ec}\gamma_e^2\Gamma=4.20\times10^6\,B\,\gamma_e^2\,\Gamma=8\times10^{11}\ {\rm Hz};\\ \nu L_\nu &\approx N_eP_{\rm syn}=\tfrac{4}{3}N_e\sigma_Tc\gamma_e^2U_B\Gamma^2=1.06\times10^{-15}\,N_e\,\gamma_e^2\,B^2\,\Gamma^2=3\times10^{43}\ {\rm erg\ s^{-1}}.\end{aligned}\qquad(1)$$

Here and below, $P_{\rm syn}$ is the total synchrotron radiation power, $\sigma_T$ is the Thomson cross

section, $U_B \equiv B^2/8\pi$ is the magnetic energy density and CGS units are used. In deriving equation (1), spherical explosion was assumed.

A third condition is the synchrotron self absorption frequency, $\nu_a \approx 2 \times 10^{11}$ Hz. For $\nu_a < \nu_m$, as is the case here, the self absorption coefficient scales as $\alpha_\nu \propto \nu^{-5/3}$ (see Rybicki & Lightman 1979, equation (6.50)), thus $\tau_\nu/\tau_{\nu_m} = \alpha_\nu/\alpha_{\nu_m} = (\nu/\nu_m)^{-5/3}$. Here, $\tau_\nu \propto \alpha_\nu$ is the optical depth, $\tau_{\nu_m} \equiv \tau_\nu(\nu = \nu_m) = \alpha_{\nu_m} R'$, and $R' = R/\Gamma$ is the co-moving size of the synchrotron emitting region. In calculating $\alpha_{\nu_m}$ we use equation (6.53) in Rybicki & Lightman (1979), which assumes power law distribution of electrons above $\gamma_e$. We use power law index $p = 2$, although the result is found not to be sensitive to neither the power law distribution assumption or the power law index; a similar result is obtained if the electrons assume a thermal distribution. Since, by definition, $\tau_{\nu_a} \equiv \tau_\nu(\nu = \nu_a) = 1$, the synchrotron self absorption frequency $\nu_a$ is

$$\frac{\nu_a^{\rm ob}}{\nu_m^{ob}} = 2.46 \times 10^{-6} N_e^{3/5} R^{-6/5} B^{-3/5} \gamma_e^{-3} \simeq \frac{1}{4} \ . \tag{2}$$

Here, the observed value of the self absorption frequency $\nu_a^{\rm ob} \approx 2 \times 10^{11}$ Hz is used.

As a fourth condition we use the assumption of ballistic expansion of the source, similar to Zauderer et al. (2011). We consider constant bulk expansion velocity of the source $\beta = (1 - \Gamma^{-2})^{1/2}$ and head-on emission. At redshift $z = 0.354$, an observed time $\Delta t^{\rm ob} = 5$ days corresponds to source frame time $\Delta t^{\rm ob}/(1+z) = 3.7$ days. Due to relativistic time compression, the actual time that the source would have expanded is $[\Delta t^{\rm ob}/(1+z)]/(1-\beta)$. Thus, the emission radius is related to the observed time by

$$R = \frac{\Delta t^{\rm ob}}{(1+z)} \cdot \frac{\beta c}{(1-\beta)} \tag{3}$$

The four constraints derived in equations (1) – (3) are insufficient to fully determine the values of the five free model parameters. We therefore choose the source size $R$ at $\Delta t^{\rm ob} = 5$ days as a free variable, and determine the values of the other four free parameters. The results of our calculation are shown in Figure 1. We present the bulk Lorentz factor $\Gamma$ (black), bulk momentum $\Gamma\beta$ (cyan), magnetic field $B$ (green), characteristic electron Lorentz factor $\gamma_e$ (red) and the number density of the radiating particles, $n_e$ (blue).

In order to constrain the allowed parameter space region, we use two additional assumptions: (1) In Fermi-type acceleration, the typical Lorentz factor of the energetic electrons $\gamma_e \leq m_p/m_e = 1836$ in the rest frame of the plasma; (2) As the emission radius is large, the magnetic field must be produced at the shock front. Thus, the ratio of magnetic energy density, $B^2/8\pi$ to the photon energy density, $L/(4\pi R^2 \Gamma^2 c)$ (often denoted by $\epsilon_B$), is smaller than unity. These constraints are shown by the dashed lines in Figure 1.

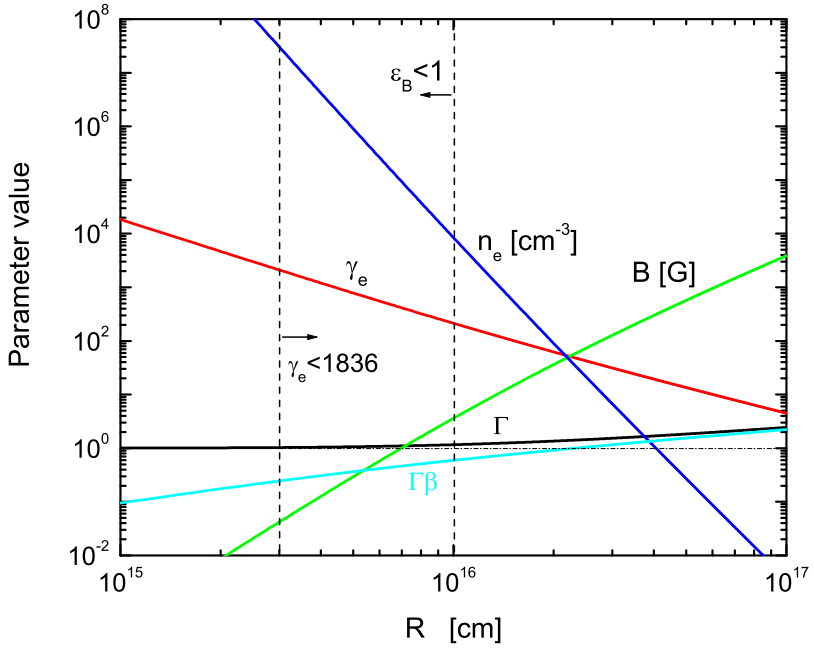


Fig. 1.— Dependence of the free model parameters: the bulk Lorentz factor, $\Gamma$ (black), the bulk momentum, $\Gamma\beta$ (cyan), the magnetic field, $B$ (green), the typical Lorentz factor of electrons, $\gamma_e$ (red) and the number density of electrons, $n_e$ (blue) on the emission radius of the radio photons, $R$, under the assumption that the radio photons originating from synchrotron emission.

After adding these two constraints, we conclude that the radio emission zone at early times fulfills the following conditions: *(i)* The emission radius is in the range $3.0 \times 10^{15}$ cm $\lesssim R \lesssim 1.0 \times 10^{16}$ cm. *(ii)* The outflow is trans-relativistic, with $1.04 \lesssim \Gamma \lesssim 1.2$, and $0.24 \lesssim \beta \lesssim 0.55$. *(iii)* The magnetic field is poorly constrained by the data, and could range from $5.0 \times 10^{-2}$ G to 7.0 G. *(iv)* The electrons are hot, with minimum random Lorentz factor exceeding $\gamma_e \gtrsim 150$. *(v)* The emitting region is dense: $3.0 \times 10^3$ cm$^{-3} < n_e < 3.0 \times 10^7$ cm$^{-3}$. This result likely excludes shocked external material as the source of the radio emission, as the typical densities (even after compressed by mild-relativistic shock waves) are much lower than these values. *(vi)* The total number of radiating particles is at the range $1.0 \times 10^{52} < N_e < 3.4 \times 10^{54}$, with likely value of $\sim 10^{53}$. We find that our results are consistent with the results derived by Zauderer et al. (2011).

### 2.2. Interpretation of early X-ray emission

Our underlying assumption is that the origin of the X-ray emission is inverse Compton (IC) scattering of the synchrotron radio photons by relativistic electrons. As we show here, these electrons must be located in a different region than the radio-emitting electrons. Following the treatment by Pe'er & Loeb (2012), two constraints can be put by the data: (I) the ratio of the IC and synchrotron peak frequencies is given by

$$\frac{\nu^{\rm ob}_{\rm peak,IC}}{\nu^{\rm ob}_{\rm peak,syn}} = \frac{4}{3}\left(\gamma_{\rm e[IC]}\Gamma\right)^2 \simeq \frac{2\times10^{18}}{8\times10^{11}}, \tag{4}$$

and, (II) the ratio of IC to synchrotron peak fluxes is

$$\frac{F_{\nu,\rm IC}}{F_{\nu,\rm syn}} = \frac{(\nu F_{\nu,peak,IC}/\nu_{\rm peak,IC})}{(\nu F_{\nu,peak,syn}/\nu_{\rm peak,syn})} = n_{e[IC]} r \sigma_{\rm T} \simeq 4\times10^{-3}. \tag{5}$$

Here, $\gamma_{e[IC]}$ and $n_{e[IC]}$ are the typical Lorentz factor and number density of electrons that emit the IC photons, and $r$ and $\Gamma$ are the typical size and the bulk Lorentz factor of the IC emission region. In estimating the ratio of the peak frequencies and fluxes, we used $\nu^{\rm ob}_{\rm peak,IC} \simeq 2\times10^{18}$ Hz, $\nu^{\rm ob}_{\rm peak,syn} \simeq 8\times10^{11}$ Hz, $\nu F_{\nu,peak,IC} \approx 3\times10^{47}$ erg s$^{-1}$, and $\nu F_{\nu,peak,syn} \approx 3\times10^{43}$ erg s$^{-1}$.

The rapid variability observed in X-rays on a time scale $\delta t^{\rm ob} \sim 100$ s constraints the size of the emitting region, $r$. While the time during which this variability is observed does not correspond directly to five days, we use it here as an order of magnitude estimate. This variability implies a relation between the emission radius of the X-rays and the bulk Lorentz factor,

$$r = \left(\frac{\delta t^{ob}}{1+z}\right)\frac{\beta c}{1-\beta} \approx 2\Gamma^2 c\frac{\delta t^{ob}}{1+z} \tag{6}$$

Equations (4), (5) and (6) exhibit three restrictive conditions provided by the observed data. As there are four free model parameters, $\Gamma$, $\gamma_{e[IC]}$, $n_{e[IC]}$ (or $N_e$) and $r$, a full solution cannot be obtained. However, we can apply a similar method to the one used in §2.1, namely take $r$ as a free parameter and obtain the values of the other three unknowns. The results of this analysis are presented in Figure 2. In this figure, we present the values of $\Gamma$ (black), $\gamma_{e[IC]}$ (red) and $n_{e[IC]}$ (blue) as a function of $r$, where $\delta t^{ob} = 100$ s is considered.

From the results of Figure 2 one can put several constraints on the X-ray emission zone: First, there is no strong constraint on the size of the emitting region, $r$. Any value in the range $10^{15}$ cm $< r < 10^{16}$ cm, which is compatible with the size of the emission zone of the synchrotron photons, is acceptable. The main constraint originate from equation (6), as large

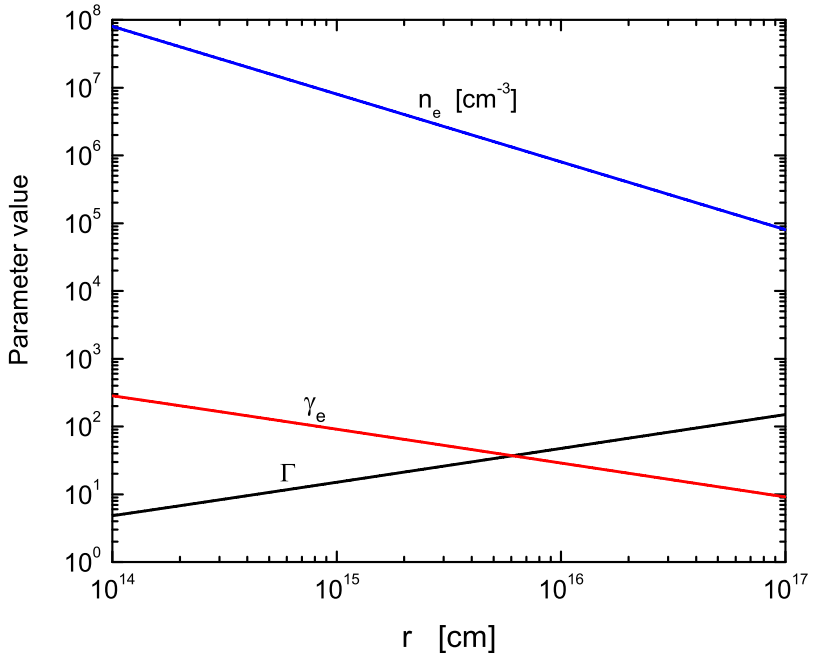


Fig. 2.— Dependence of the free model parameters of the X-ray emitting region: the bulk Lorentz factor, $\Gamma$ (black) the typical Lorentz factor of electrons, $\gamma_e$ (red) and the number density of electrons, $n_e$ (blue) on the radius of source, $r$. We assume that IC scattering of the radio photons are the main source of X-rays.

radius implies large bulk Lorentz factor, as $\Gamma \simeq R^{1/2}/(2.1 \times 10^6)$. Thus, value of $r \approx 10^{16}$ imply $\Gamma \approx 50$, much larger than the value obtained for the radio emission zone. Even value of $r = 10^{15}$ cm implies $\Gamma \approx 15$, inconsistent with the finding for the radio emitting zone. Thus, while the size of the radio and X-ray emitting regions can be comparable, the X-ray emitting region must propagate at much larger Lorentz factor than the radio emitting region. Second, the IC emitting electrons are not as hot as the radio emitting electrons. For $r \gtrsim 10^{15}$ cm, $\Gamma \gtrsim 15$, which, using equation (4) imply $\gamma_{e[IC]} \lesssim 100$. Third, the number density of the radiating electrons, $10^4\,\mathrm{cm}^{-3} \lesssim n \lesssim 10^8\,\mathrm{cm}^{-3}$ is comparable to the number density of the radio emitting particles, and is thus likely too high to be explained by compression of the external material. A similar conclusion holds for the total number of the radiating particles.

Thus, we conclude that while the two emission regions can have a comparable size, the X-ray emission zone must have a much larger Lorentz factor than the radio emission zone; moreover, the electrons in the X-ray emitting region must be colder than the electrons that

emit at radio frequencies. Alternatively, the bulk motion may be similar, but only if the X-ray emitting region is at much smaller distance, $10^{12.5}$ cm. These results are summarized in Table 1.

Table 1: Summary of key properties of both radio and X-ray emission zones of Swift J164449.3+573451

| | $R\,[\mathrm{cm}]$ | $\Gamma$ | $\gamma_e$ | $n_e\,[\mathrm{cm}^{-3}]$ | $N_e$ |
|---|---|---|---|---|---|
| Radio emission zone | $3\times10^{15}-10^{16}$ | $\lesssim 1.2$ | $150-2000$ | $10^{3.5}-10^{7.5}$ | $10^{52}-10^{54.5}$ |
| X-ray emission zone | $10^{15}-10^{16}$ | $15-50$ | $30-100$ | $10^{6}-10^{8}$ | $10^{52.5}-10^{54.5}$ |
| (alternative) | $10^{12.5}$ | $\lesssim 1.2$ | $\sim 1000$ | $10^{9.5}$ | $10^{47.5}$ |

Notes. — In the table, the model parameters $R$: source radius, $\Gamma$: bulk Lorentz factor, $\gamma_e$: typical Lorentz factor of relativistic electrons, $n_e$: number density of emitting electrons, and $N_e$: total number of electrons.

Similarly, although order-of-magnitude variations in brightness are seen in the X-rays, the detailed radio light curve does not reveal the coincident variations that would be expected for SSC (Zauderer et al. 2011; Levan et al. 2011). We therefore conclude that the X-ray emission must originate from a region separated than the radio emission region.

While observations made in the first few days cannot discriminate between the two alternatives for the X-ray emitting region, we show in §3 below that the re-brightening observed at radio flux after tens of days can be naturally explained as resulting from material collected by the X-ray emitting plasma, provided that it travels at $\Gamma \approx 10-20$. Thus, the first model, in which the X-ray emission region is separated from the radio emission region *in velocity space* is preferred. This leads us to a proposed *two component jet*, in which the fast, X-ray emitting material, is surrounded by a slower, radio emitting material. A cartoon demonstrating this model is shown in Figure 3.

## 3. Late time radio evolution

The two component jet model presented above has a distinct prediction. As the plasma expands into the interstellar material (ISM), it collects material, slows and cools. This situation is similar to the afterglow phase in GRBs. Thus, using similar assumptions, one can predict the late time synchrotron emission from the decelerating plasma. One notable difference from GRB afterglow, though, is that the X-ray emitting plasma is mildly rela-

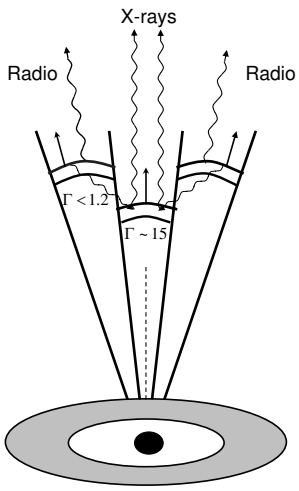


Fig. 3.— Sketch of geometrical configuration and emission regions for TDE Swift 1644+57. The inner jet has a Lorentz factor $\Gamma \approx 15$, and is responsible for the early times X-ray emission. The outer jet has Lorentz factor $\lesssim 1.2$, and is the source of the early times radio emission. As the inner jet propagates through the ISM it collects material and cools. Synchrotron emission from the collected material is the source of the re-brightening seen in radio frequencies after $\approx 30$ days.

tivistic, while the radio emitting plasma is trans-relativistic. Thus, when calculating the dynamics, one cannot rely on the ultra-relativistic scheme (Blandford & McKee 1976), but has to consider the transition to the Newtonian regime.

### 3.1. Dynamics and radiation from an expanding jet

The dynamics of plasma expanding through the ISM is well studied in the literature (Blandford & McKee 1976; Katz & Piran 1997; Chiang & Dermer 1999; Piran 1999; Huang et al. 1999; van Paradijs et al. 2000; Pe'er 2012; Nava et al. 2012). Here we briefly review the basic theory, which we then utilize in calculating the expected late time radio emission from TDE Swift 1644+57.

We assume that by the relevant times (tens of days), the reverse shock had crossed the plasma, and thus only the forward shock exists. The evolution of the bulk Lorentz factor of

the expanding plasma is given by (Pe'er 2012)

$$\frac{\mathrm{d}\Gamma}{\mathrm{d}m} = -\frac{\hat{\gamma}\left(\Gamma^2-1\right)-\left(\hat{\gamma}-1\right)\Gamma\beta^2}{M+\epsilon m+\left(1-\epsilon\right)m\left[2\hat{\gamma}\Gamma-\left(\hat{\gamma}-1\right)\left(1+\Gamma^{-2}\right)\right]}. \tag{7}$$

Here, $M$ is the mass of the ejected matter, $m$ is the mass of the collected ISM, $\Gamma$ is the bulk Lorentz factor of the flow, $\hat{\gamma}$ is the adiabatic index and $\epsilon$ is the fraction of the shock-generated thermal energy that is radiated ($\epsilon = 0$ in the adiabatic case and $\epsilon = 1$ in the radiative case). Note that equation (7) holds for any value of $\Gamma$, both in the ultra-relativistic ($\Gamma \gg 1$) and the sub-relativistic ($\beta \ll 1$) limits.

Under the assumption of constant ISM density, the collected ISM mass is related to the distance $\mathrm{d}R$ and observed time $\mathrm{d}t$ via

$$\begin{aligned} \mathrm{d}m &= 4\pi R^2 n_{\rm ISM} m_{\rm p} \mathrm{d}R; \\ \mathrm{d}R &= \Gamma\beta c\left(\Gamma+\Gamma\beta\right)\mathrm{d}t = \tfrac{\beta}{1-\beta} c\mathrm{d}t, \end{aligned} \tag{8}$$

where $m_p$ is the proton's rest mass and $n_{\rm ISM}$ is the ISM density. In deriving the second line in equation (8), we have explicitly assumed that the observed photons are emitted from a plasma that propagates towards the observer. A more comprehensive calculation which considers the integrated emission from different angles to the line of sight results in a similar solution, up to a numerical factor of a few (Waxman 1997; Pe'er & Wijers 2006).

In order to predict the synchrotron emission, one needs to calculate the magnetic field, $B$ and characteristic electron's Lorentz factor, $\gamma_{\rm el}$. This calculation is done as follows. By solving the shock jump conditions, one gets the energy density behind the shock (Blandford & McKee 1976),

$$u_2 = \left(\Gamma-1\right)\frac{\hat{\gamma}\Gamma+1}{\hat{\gamma}-1} n_{\rm ISM} m_{\rm p} c^2 \ . \tag{9}$$

Equation (9) is exact for any velocity, including both the ultra-relativistic and the Newtonian limits. A useful approximation for the adiabatic index is $\hat{\gamma} = (4\Gamma+1)/(3\Gamma)$ (e.g., Dai et al. 1999)[1]. In the ultra-relativistic limit, $\Gamma \gg 1$, $\hat{\gamma} = 4/3$ and equation (9) takes the form $u_2 \approx 4\Gamma^2 n_{\rm ISM} m_{\rm p} c^2$; While in the Newtonian limit, $\beta \ll 1$ and $\hat{\gamma} = 5/3$, equation (9) becomes $u_2 \approx 2\beta^2 n_{\rm ISM} m_{\rm p} c^2$.

The shock-generated magnetic field assumes to carry a fraction $\epsilon_{\rm B}$ of the post-shock thermal energy, $B^2/8\pi = \epsilon_{\rm B} u_2$,

$$B = \begin{cases} \left(32\pi\epsilon_{\rm B} n_{\rm ISM} m_{\rm p} c^2\right)^{1/2}\Gamma & \text{(relativistic limit)}, \\ \left(16\pi\epsilon_{\rm B} n_{\rm ISM} m_{\rm p} c^2\right)^{1/2}\beta & \text{(Newtonian limit)}. \end{cases} \tag{10}$$

[1]A more accurate formula appears in Pe'er (2012).

Similarly, a constant fraction $\epsilon_{\rm e}$ of the post-shock thermal energy is assumed to be carried by energetic electrons, resulting in $\gamma_{\rm el} m_{\rm e} c^2 = \epsilon_{\rm e}(u_2/n_2)$, where the number density in the shocked region is $n_2 = n_{\rm ISM}(\hat{\gamma}\Gamma + 1)/(\hat{\gamma} - 1)$. This leads to

$$\gamma_{\rm el} = \begin{cases} \epsilon_{\rm e}\Gamma\left(\frac{m_{\rm p}}{m_{\rm e}}\right) & \text{(relativistic limit)}, \\ \epsilon_{\rm e}\frac{\beta^2}{2}\left(\frac{m_{\rm p}}{m_{\rm e}}\right) & \text{(Newtonian limit)}. \end{cases} \tag{11}$$

In order to calculate the observed peak frequency and flux, we discriminate between two cases:

(i) In the *optically thin* emission, $\nu_a < \nu_m$, i.e., $\tau_{\nu_m} < 1$, the peak synchrotron frequency is $\nu_p^{\rm ob} = \nu_m^{\rm ob} = (3/4\pi)(q_e B/m_e c)\gamma_{\rm el}^2\Gamma$ and the peak flux $F_{\nu_p} = F_{\nu_m} \approx (N_e/4\pi d_L^2)(2\sigma_T m_e c^2 B\Gamma/9q_e)$ (e.g., Sari et al. 1998). Here, $d_L$ is the luminosity distance and $N_e \propto R^3$ is the total number of radiating electrons (originating both at the explosion, as well as collected ISM). In the limit where the total number of swept-up ISM material is much larger than the original ejected material, analytic scaling laws can be obtained in the ultra-relativistic and Newtonian limits. In the relativistic regime, $\Gamma \gg 1$, $\Gamma \propto t^{-3/8}$ and $R \propto t^{1/4}$, and thus $\nu_p^{\rm ob} \propto t^{-3/2}$ and $F_{\nu_p} \propto t^0$. On the other hand, in the Newtonian limit, $\beta \propto t^{-3/5}$ and $R \propto t^{2/5}$, one finds $\nu_p^{\rm ob} \propto t^{-3}$ and $F_{\nu_p} \propto t^{3/5}$.

(ii) In the *optically thick* regime, $\nu_a > \nu_m$, i.e., $\tau_{\nu_m} > 1$, the observed peak frequency $\nu_p$ and the peak flux $F_{\nu_p}$ are at the self absorption frequency, $\nu_a$. For a power law distribution of electrons above $\gamma_{\rm el}$ with power law index $p$, these are given by

$$\begin{aligned} \nu_p^{\rm ob} = \nu_a^{\rm ob} = \nu_m^{\rm ob}\tau_{\nu_m}^{2/(p+4)} &= \tfrac{3}{4\pi}\tfrac{q_e B}{m_e c}\gamma_{\rm el}^2\Gamma\tau_{\nu_m}^{2/(p+4)} \ , \\ F_{\nu_p} = F_{\nu_m}\left(\tfrac{\nu_a}{\nu_m}\right)^{-\frac{p-1}{2}} &= F_{\nu_m}\tau_{\nu_m}^{-\frac{p-1}{p+4}} \approx \tfrac{N_{\rm e}}{4\pi {\rm d}_{\rm L}^2}\tfrac{2}{9}\tfrac{\sigma_{\rm T} m_{\rm e} c^2}{q_e} B\Gamma\tau_{\nu_m}^{-\frac{p-1}{p+4}} \ . \end{aligned} \tag{12}$$

The optical depth at $\nu_m$, $\tau_{\nu_m}$ is calculated as follows. We first point out that the comoving number density of the electrons in the shocked plasma frame is $n_2 \simeq 4\Gamma n_{\rm ISM}$.[2] Using equation (6.52) in Rybicki & Lightman (1979), we find that $\tau_{\nu_m} = \alpha_{\nu_m}(R/\Gamma) = f(p) n_{\rm ISM} B^{-1}\gamma_{\rm el}^{-5} R$ (see also Pe'er & Waxman 2004). Here, $f(p) = (p-1)(8\pi\sqrt{3}q_e/9)2^{p/2}\Gamma((2p+2)/12)\Gamma((3p+22)/12)$ is a function of the power law index, $p$ of the accelerated electrons above $\gamma_{\rm el}$, and $\Gamma(x)$ is $\Gamma$ function of argument $x$. Using this result in equation (12), one can obtain analytic scaling laws for the temporal evolution of $\nu_p^{\rm ob}$ and $F_{\nu_p}$ in both the ultra-relativistic and Newtonian limits, in a similar way to the derived expressions in the optically thin limit above. In the relativistic regime, $\nu_p^{\rm ob} \propto t^{-(3p+2)/2(p+4)} \propto t^{-2/3}\,(p=2)$ and $F_{\nu_p} \propto t^{5(1-p)/2(p+4)} \propto$

[2]The equation relating the downstream ($n_2$) and upstream ($n_1$) number densities, $n_2 = (\hat{\gamma}\Gamma+1)n_1/(\hat{\gamma}-1)$ holds for any strong shock, at any velocity, both in the relativistic and Newtonian regimes.

$t^{-5/12}\,(p=2)$. In the Newtonian limit, one finds $\nu_p^{\rm ob} \propto t^{(2-3p)/(p+4)} \propto t^{-2/3}\,(p=2)$ and $F_{\nu_p} \propto t^{(47-32p)/5(p+4)} \propto t^{-17/30}\,(p=2)$.

### 3.2. Radiative cooling of the electrons

In the calculation presented in §3.1 (in particular, equation (11) above), we considered heating of the ISM plasma as it crosses the shock front. Once the ISM particles cross the shock front, they lose their energy by radiative cooling. Hence, their typical Lorentz factor $\gamma_{\rm el}$ decreases with time. Similarly, the original ejected material from the tidally disrupted star cools with time.

Within the context of our double jet model, this cooling has a more pronounced effect on the lightcurve originating from the outer jet, that is responsible for the early time radio emission. This is because this region is composed of a dense plasma, that propagates at trans-relativistic velocities (see Table 1). Thus, the contribution of the swept-up ISM material to the emission during the first $\sim$ month from this region is minor, as opposed to the contribution of the collected ISM to the emission from the inner jet. This can be seen by noting that during Newtonian expansion, $R \propto t^{2/5}$. Thus, between five and thirty days, the radius of the radio emitting region is increased by a factor $\approx 2$, and therefore cannot exceed $\approx 2\times10^{16}$ cm. As a result, unless the ISM density is much larger than $\sim 10^3\,{\rm cm}^{-3}$, contribution from the collected ISM to the emission from the outer jet is subdominant.

The radio emitting electrons cool due to synchrotron and inverse Compton scattering. The radiated power from a relativistic electron with Lorentz factor $\gamma_{\rm el}$ is $P = P_{\rm syn} + P_{\rm IC} = (4/3)c\sigma_T\,(U_B + U_{\rm ph})\,\gamma_{\rm el}^2$, where $U_B$ and $U_{\rm ph}$ are the magnetic and radiative field energy densities, respectively.

Both $U_B$ and $U_{\rm ph}$ decrease with radius (and time). As discussed in §3.1 above, during the Newtonian expansion phase $B \propto \beta \propto t^{-3/5}$ (see equation (10)), and thus $U_B \propto t^{-6/5}$. Similarly, $U_{\rm ph} = L/(4\pi R^2\Gamma^2 c)$, where the luminosity is $L \propto N_e\gamma_{\rm el}^2 B^2\Gamma^2 \propto \beta^6 \propto t^{-18/5}$ (assuming that most radiative particles are from the original ejecta). This leads to $U_{\rm ph} \propto t^{-22/5}$, namely the IC component decreases much faster than the synchrotron component.

We can therefore write $P \approx (4/3)c\sigma_T U_{B,0}(t/t_0)^{-6/5}\gamma_{\rm el}^2$, where $U_{B,0}$ is the magnetic field energy density at fiducial time, $t_0$ which is taken in the calculations below to be five days (observed time). The characteristic particles Lorentz factor at any given time $t > t_0$ is given by

$$\gamma_{\rm el}(t) = \frac{\gamma_{\rm el,0}}{1 + \frac{20}{3}\frac{\sigma_T}{m_e c}U_{B_0}\gamma_{\rm el,0}t_0\left[1-(t/t_0)^{-1/5}\right]}\ , \tag{13}$$

where $\gamma_{\rm el,0}$ is the electron's Lorentz factor at $t_0$. The temporal evolution of the electron's Lorentz factor and the decay law of the magnetic field allow calculation of the late time evolution of both the peak radio frequency and peak radio flux from the outer jet region.

## 4. Interpretation of the late time radio emission of Sw J1644+57

The temporal evolution of the radio flux and peak radio frequency of Sw J1644+57 up to 216 days from the initial outburst are presented in Figures 4, 5 (data taken from Berger et al. 2012). Three separate regimes are identified in both figures: (I) At early times, $\lesssim 30$ days, the flux decreases from $\sim 40$ mJy at $\sim 5$ days to $\sim 15$ mJy at $\sim 30$ days. During this period, $\nu_p^{\rm ob}$ rapidly decays, with a decay law consistent with $\nu_p^{\rm ob} \propto t^{-\alpha}$ and $\alpha \approx 2.0$. (II) Between $30 - 100$ days, the flux *increases* by a factor of $\sim 1.8$ (from $\sim 20$ mJy to $\sim 35$ mJy). At the beginning of this epoch, at $t^{\rm ob} \sim 30 - 45$ days, the radio peak frequency $\nu_p^{\rm ob}$ increases by a factor of a $few$, while during the rest of this epoch it shows a similar decay law as is seen at early times, $\nu_p^{\rm ob} \propto t^{-\alpha}$ with $\alpha \approx 2.0$. (III) Finally, at very late times, $\gtrsim 100$ days, the flux decays again. This decay is accompanied by a slow decay in the peak radio frequency, much slower than the decay observed at earlier phases. We point out that the increase in the radio flux observed at epoch (II) led Berger et al. (2012) to suggest that late time central engine activity may take place.

Based on the discussion presented in the previous sections, we suggest the following interpretation to the late time radio emission of Sw J1644+57: (I) During the early decay phase, $t^{\rm ob} < 30$ days, the emission is dominated by synchrotron radiation from the same electrons that emitted the radio emission at early times; this is the outer jet component in our model (see Figure 3). This emission is thus a continuation of the emission observed at early times. The observed decay of both the flux and peak frequency is due to the decreasing of magnetic field and the radiative cooling of these electrons. (II) At $t^{\rm ob} \approx 30$ days, there is a transition: the inner jet plasma, that originally emitted the X-ray photons, expands into the ISM, collects ISM material and cools. At this time, synchrotron emission from this plasma becomes the dominant component at radio frequencies. Initially, the inner jet propagates at relativistic speeds, with $\Gamma \gtrsim 15$ (see discussion in §2.2 and Table 1). However, as it propagates into the ISM, the plasma collects material from the surrounding ISM and slows; the collected material contributes to the radio emission, resulting in an increase in the radio flux. (III) Finally, at $t^{\rm ob} \sim 100$ days, the emission becomes optically thick (self absorption frequency is larger than the peak frequency), which causes the late time decay.

Fits to the temporal evolution of the peak radio frequency and peak flux are shown in Figures 4 and 5. In producing these fits, we use the following parameters, which match the

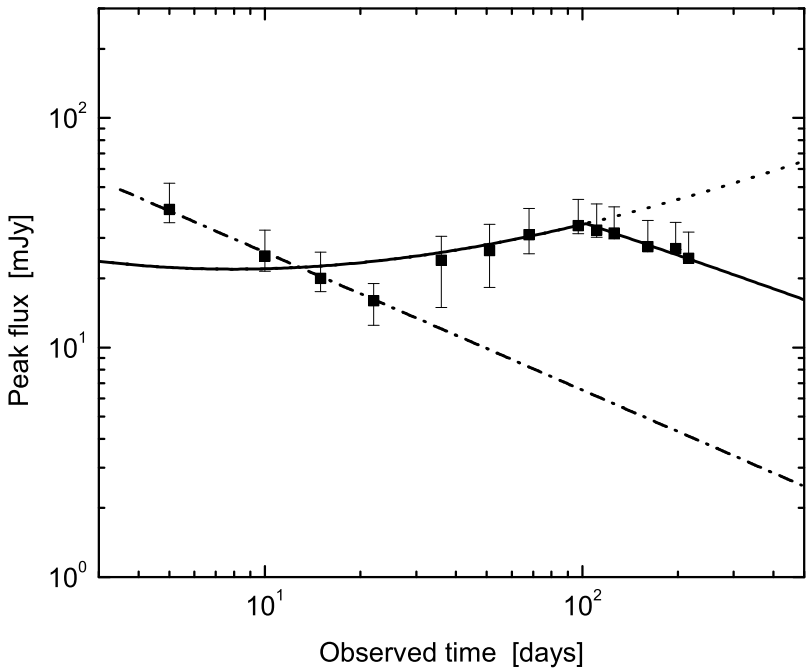


Fig. 4.— Temporal evolution of peak flux of the radio emission of Swift 1644+57. Data is taken from Berger et al. (2012). Dash-dotted line is the contribution of the outer (slower) jet, while solid and dotted lines are the contribution from the inner (faster) jet. As the inner jet propagates into the ISM, it collects material and cools; thus, after $\sim 30$ days, radio emission from this region dominates the radio flux. At $\sim 100$ days, the peak flux enters the optically thick regime ($\tau_{\nu_p} > 1$), which causes the decay see at these times. The values of the free model parameters used are presented in the text.

early and late time properties of the flow. For the outer jet, we use initial expansion radius (at observed time $t_0^{\rm ob} = 5$ days) $R_0 = 10^{16}$ cm. The typical electron's Lorentz factor is taken to be $\gamma_{\rm el,0} = 190$, magnetic field $B_0 = 4.5$ G, and initial bulk Lorentz factor $\Gamma(t_0^{\rm ob}) \simeq 1.18$. These values correspond to $\epsilon_{\rm e} \approx 0.58$ and $\epsilon_{\rm B} \approx 0.13$, and imply total number of radiating particles $N_e(t_0) = 1.25 \times 10^{53}$. These values are consistent with the findings in §2.1 (see Table 1). These parameters result in initial peak synchrotron frequency $\nu_{p,0}^{\rm ob} = 8.0 \times 10^{11}$ Hz, and peak observed flux $F_{\nu_p,0} = 39.4$ mJy.

For the inner jet, we find that the best fit is obtained when using initial bulk Lorentz factor $\Gamma(t_0^{\rm ob}) = 17$, $\epsilon_{\rm e} = 0.54$, $\epsilon_{\rm B} = 0.54$ and $r(t_0^{\rm ob}) \simeq 1.2 \times 10^{15}$ cm. We point out that the value of $\epsilon_B$ is not constrained by early X-ray data. Moreover, here the collected ISM plays

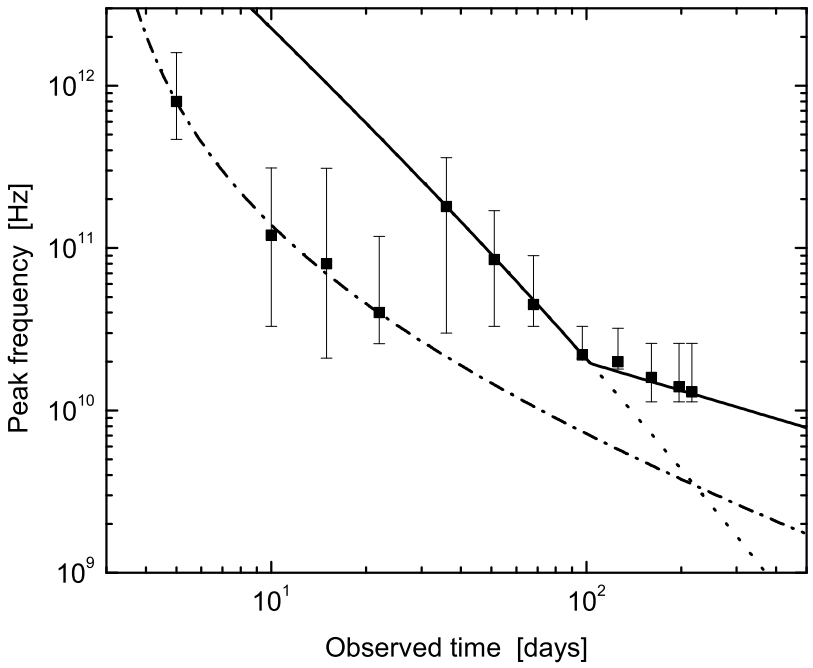


Fig. 5.— Temporal evolution of peak frequency for the radio emission of Swift 1644+57. Observed data taken from Berger et al. (2012). Lines have the same meaning as in Figure 4. Three distinctive regimes are clearly seen.

a significant role. Thus, we could constrain the ISM density to be $n_{\rm ISM} = 2.7$ cm$^{-3}$. We further assume that the shocked ISM have a power law distribution above $\gamma_{\rm el}$ with power law index $p = 2$. When calculating the dynamics in equation (7), we consider adiabatic expansion, namely $\epsilon = 0$.

As the inner jet propagates into the ISM it collects material and slows. Using Equations 7, 8, we find that at observed time $t^{\rm ob} = 100$ days, it reaches radius $R \sim 6.0 \times 10^{17}$ cm, with bulk Lorentz factor $\Gamma \sim 1.15$. At this time, the magnetic field is $B \sim 0.19$ G and the characteristic electrons Lorentz factor is $\gamma_{\rm el} \approx 150$. This result in $\nu_p^{\rm ob} = 2.06 \times 10^{10}$ Hz and $F_{\nu_p} = 34.4$ mJy. However, at this time, $\tau_{\nu_p} \approx 1$, which implies that from this time onward synchrotron radiation is in the *optically thick* regime, and its late time properties are described by equations (12). While the dotted line in in Figures 4, 5 presents the model fits in the optically thin regime, the solid line in these figures represent the expected peak frequency and flux in the optically thin region at early times, and optically thick regions at $t^{\rm ob} > 100$ days.

## 5. Conclusions and Discussions

In this paper, we studied the early and late time emission of the TDE Sw J1644+57, both at radio and X-ray frequencies. Based on our analysis, we propose a two-component jet model (see Figure 3) that fits the observations. Our model explains, for the first time, *both* the early time X-ray and radio emission, as well as the complex late time radio behavior.

By analyzing the early time ($t^{\rm ob} \lesssim 5$ days) data, we conclude that the radio and X-ray photons must have separate origins (see §2, Table 1). We are able to put strong constraints on the properties of the radio emitting plasma (see §2.1 and Figure 1), and somewhat weaker constraints on the properties of the X-ray emitting plasma (§2.2 and Figure 2). Stronger constraints on the *initial* properties of the X-ray emitting plasma are obtained when considering late time radio emission.

Our jet within a jet model naturally explains the complex temporal evolution of the radio emission at late times (up to $\gtrsim 200$ days). We solved in §3 the dynamics and expected radiation from the jet propagating into the ISM. We stress that as the initial Lorentz factor of the inner jet is mild (our best fit gives $\Gamma \approx 17$), one has to consider the transition between the relativistic and the Newtonian expansion phases, and cannot rely on analysis of ultra-relativistic outflows, as is the case in GRBs. We further consider the radiative cooling of particles behind the shock front.

We demonstrated how our model can be used to fit the data in §4. Our key idea is that the observed signal can be split into three separate regions: at early times, radio emission is dominated by the outer jet. The decay of the peak frequency and flux is attributed to radiative cooling of the electrons and the declining of magnetic field. Between $30-100$ days, the radio emission is dominated by the inner jet, in the optically thin regime. The inner jet propagates at relativistic speeds and collects material from the surrounding ISM. The addition of the collected material results in the increase of radio flux. Finally, at very late time, $t^{\rm ob} \gtrsim 100$ days, the radio emission is dominated by the inner jet, in the *optically thick* regime. This causes the observed late time decay of peak flux and frequency.

When analyzing the early time data, we use the common interpretation of the radio emission as originating from synchrotron radiation. We find that the bulk Lorentz factor of the synchrotron emitting plasma is $\Gamma \lesssim 1.2$. Our analysis method is similar to that used by Zauderer et al. (2011), albeit being more general, as we avoid the equipartition assumption used in that work. The X-ray emission is interpreted as IC scattering of the radio photons, however our analysis indicates that the bulk motion of the X-ray emitting region is much higher, $\Gamma \gtrsim 15$; alternatively, the emission radius is much smaller, $r \sim 10^{12.5}$ cm. We thus conclude that radio and X-ray emission zones are completely separated, either spatially or

in velocity space. This is consistent with the separate temporal behavior observed at early times, as the observed X-rays maintained a more constant level after the first 48 hours (albeit with episodic brightening and fading spanning more than an order of magnitude in flux; see Levan et al. 2011), whereas the low frequency emission decreased markedly.

Our calculated X-ray luminosity can match the observed X-ray luminosity of TDE Sw J1644+57, $L_X \approx 10^{47.5}$ erg sec$^{-1}$, exceeding the radio emission by a factor $\sim 10^3 - 10^4$. If the emission is isotropic, the X-ray luminosity of Sw J1644+57 corresponds to the Eddington luminosity of an $\sim 10^9\ M_\odot$ MBH, which is incompatible with the upper limit $\sim 10^7\ M_\odot$ of the MBH mass derived from variability (Bloom et al. 2011; Burrows et al. 2011), so the source is required to be relativistically beamed. We have obtained the bulk Lorentz factor of the relativistic jetted outburst $\Gamma \sim 15$, which is very close to the typical value inferred in blazars. Therefore, if the beaming angle of the jet $\theta_j \approx 1/\Gamma \sim 0.1$, the beaming-corrected luminosity $f_{\rm b} L_X \sim 10^{45}$ erg sec$^{-1}$ ($f_{\rm b} = (1 - \cos\theta_j)$ is the beaming factor) becomes consistent with the Eddington luminosity of a $\sim 10^7\ M_\odot$ MBH (see also Bloom et al. 2011).

Berger et al. (2012) present the continued radio observations of the TDE Sw J1644+57 extending to $\sim 216$ days. In their work, they fitted the data using the model of Granot & Sari (2002), and concluded that the re-brightening seen after $\sim 30$ days cannot be explained in the framework of that model. They thus conclude that an increase in the energy by about an order of magnitude is required. As discussed above, the re-brightening is very natural in our scenario due to the increase in the collected material when the jetted outburst propagates through the ISM.

The idea of jet within a jet was suggested in the past as a way to explain the morphology of high energy emission from active galactic nuclei (AGNs) (Ghisellini et al. 2005; Hardcastle 2006; Jester et al. 2006; Siemiginowska et al. 2007), and in the context of GRBs in explaining the break observed in the afterglow light curve (Racusin et al. 2008; de Pasquale et al. 2009; Filgas et al. 2011), as well as some of the properties of the prompt emission (Lundman et al. 2012). While the theory of jet launching is still incomplete, clearly, jets, being collimated outflows are expected have lateral velocity gradient. The analysis done here suggests that such a velocity gradient exists in jets originating from TDEs. In principle, the outer jet may also represent a cylindrical boundary layer owing to the interaction of the inner jet with the ambient gas.

While Sw J1644+57 is the first TDE event from which the existence of relativistic jets is inferred, and the most widely discussed one in this context, it is possible that other such events were detected. Recently, Cenko et al. (2012) reported a second event, Sw J2058.4+0516 which is a potential candidate for a relativistic flare. While currently, no late time radio lightcurve is currently available, we can predict that if such a lightcurve

becomes available it should show the same complex behavior of Sw J1644+57.

We are grateful to Bevin A. Zuderer and Brian D. Metzger for useful discussions. DL acknowledges support by the National Science Foundation of China (Grant Nos. 11078014 and 11125313), the National Basic Research Program of China (Grant No. 2009CB824904), and the Shanghai Science and Technology Commission (Program of Shanghai Subject Chief Scientist; Grant No. 12XD1406200). This work was supported in part by NSF grant AST-0907890 and NASA grants NNX08AL43G and NNA09DB30A. AP acknowledges support from Fermi GI program #41162.

## REFERENCES

Berger, E., Levan, A., Tanvir, N. R., Zauderer, A., Soderberg, A. M., & Frail, D. A. 2011, GRB Coordinates Network, 11854, 1

Berger, E., Zauderer, A., Pooley, G. G., Soderberg, A. M., Sari, R., Brunthaler, A., & Bietenholz, M. F. 2012, ApJ, 748, 36

Blandford, R. D. & McKee, C. F. 1976, Physics of Fluids, 19, 1130

Bloom, J. S., Giannios, D., Metzger, B. D., Cenko, S. B., Perley, D. A., Butler, N. R., Tanvir, N. R., Levan, A. J., O'Brien, P. T., Strubbe, L. E., De Colle, F., Ramirez-Ruiz, E., Lee, W. H., Nayakshin, S., Quataert, E., King, A. R., Cucchiara, A., Guillochon, J., Bower, G. C., Fruchter, A. S., Morgan, A. N., & van der Horst, A. J. 2011, Science, 333, 203

Bogdanović, T., Eracleous, M., Mahadevan, S., Sigurdsson, S., & Laguna, P. 2004, ApJ, 610, 707

Burrows, D. N., Kennea, J. A., Ghisellini, G., Mangano, V., Zhang, B., Page, K. L., Eracleous, M., Romano, P., Sakamoto, T., Falcone, A. D., Osborne, J. P., Campana, S., Beardmore, A. P., Breeveld, A. A., Chester, M. M., Corbet, R., Covino, S., Cummings, J. R., D'Avanzo, P., D'Elia, V., Esposito, P., Evans, P. A., Fugazza, D., Gelbord, J. M., Hiroi, K., Holland, S. T., Huang, K. Y., Im, M., Israel, G., Jeon, Y., Jeon, Y.-B., Jun, H. D., Kawai, N., Kim, J. H., Krimm, H. A., Marshall, F. E., P. Mészáros, Negoro, H., Omodei, N., Park, W.-K., Perkins, J. S., Sugizaki, M., Sung, H.-I., Tagliaferri, G., Troja, E., Ueda, Y., Urata, Y., Usui, R., Antonelli, L. A., Barthelmy, S. D., Cusumano, G., Giommi, P., Melandri, A., Perri, M., Racusin, J. L., Sbarufatti, B., Siegel, M. H., & Gehrels, N. 2011, Nature, 476, 421

Cao, D. & Wang, X.-Y. 2012, ArXiv e-prints

Cenko, S. B., Krimm, H. A., Horesh, A., Rau, A., Frail, D. A., Kennea, J. A., Levan, A. J., Holland, S. T., Butler, N. R., Quimby, R. M., Bloom, J. S., Filippenko, A. V., Gal-Yam, A., Greiner, J., Kulkarni, S. R., Ofek, E. O., Olivares E., F., Schady, P., Silverman, J. M., Tanvir, N. R., & Xu, D. 2012, ApJ, 753, 77

Chiang, J. & Dermer, C. D. 1999, ApJ, 512, 699

Dai, Z. G., Huang, Y. F., & Lu, T. 1999, ApJ, 520, 634

De Colle, F., Guillochon, J., Naiman, J., & Ramirez-Ruiz, E. 2012, ApJ, 760, 103

de Pasquale, M., Evans, P., Oates, S., Page, M., Zane, S., Schady, P., Breeveld, A., Holland, S., Kuin, P., Still, M., Roming, P., & Ward, P. 2009, MNRAS, 392, 153

Evans, C. R. & Kochanek, C. S. 1989, ApJ, 346, L13

Filgas, R., Krühler, T., Greiner, J., Rau, A., Palazzi, E., Klose, S., Schady, P., Rossi, A., Afonso, P. M. J., Antonelli, L. A., Clemens, C., Covino, S., D'Avanzo, P., Küpcü Yoldaş, A., Nardini, M., Nicuesa Guelbenzu, A., Olivares, F., Updike, E. A. C., & Yoldaş, A. 2011, A&A, 526, A113

Fruchter, A., Misra, K., Graham, J., Levan, A., Tanvir, N., & Bloom, J. 2011, GRB Coordinates Network, 11881, 1

Ghisellini, G., Tavecchio, F., & Chiaberge, M. 2005, A&A, 432, 401

Giannios, D. & Metzger, B. D. 2011, MNRAS, 416, 2102

Granot, J. & Sari, R. 2002, ApJ, 568, 820

Guillochon, J., Ramirez-Ruiz, E., Rosswog, S., & Kasen, D. 2009, ApJ, 705, 844

Hardcastle, M. J. 2006, MNRAS, 366, 1465

Hills, J. G. 1975, Nature, 254, 295

Huang, Y. F., Dai, Z. G., & Lu, T. 1999, MNRAS, 309, 513

Jester, S., Harris, D. E., Marshall, H. L., & Meisenheimer, K. 2006, ApJ, 648, 900

Katz, J. I. & Piran, T. 1997, ApJ, 490, 772

Krolik, J. H. & Piran, T. 2011, ApJ, 743, 134

Levan, A. J., Tanvir, N. R., Cenko, S. B., Perley, D. A., Wiersema, K., Bloom, J. S., Fruchter, A. S., Postigo, A. d. U., O'Brien, P. T., Butler, N., van der Horst, A. J., Leloudas, G., Morgan, A. N., Misra, K., Bower, G. C., Farihi, J., Tunnicliffe, R. L., Modjaz, M., Silverman, J. M., Hjorth, J., Thöne, C., Cucchiara, A., Cerón, J. M. C., Castro-Tirado, A. J., Arnold, J. A., Bremer, M., Brodie, J. P., Carroll, T., Cooper, M. C., Curran, P. A., Cutri, R. M., Ehle, J., Forbes, D., Fynbo, J., Gorosabel, J., Graham, J., Hoffman, D. I., Guziy, S., Jakobsson, P., Kamble, A., Kerr, T., Kasliwal, M. M., Kouveliotou, C., Kocevski, D., Law, N. M., Nugent, P. E., Ofek, E. O., Poznanski, D., Quimby, R. M., Rol, E., Romanowsky, A. J., Sánchez-Ramírez, R., Schulze, S., Singh, N., van Spaandonk, L., Starling, R. L. C., Strom, R. G., Tello, J. C., Vaduvescu, O., Wheatley, P. J., Wijers, R. A. M. J., Winters, J. M., & Xu, D. 2011, Science, 333, 199

Loeb, A. & Ulmer, A. 1997, ApJ, 489, 573

Lundman, C., Pe'er, A., & Ryde, F. 2012, ArXiv e-prints

Meszaros, P. & Rees, M. J. 1993, ApJ, 405, 278

Metzger, B. D., Giannios, D., & Mimica, P. 2012, MNRAS, 420, 3528

Mïller, J. M. & Gültekin, K. 2011, ApJ, 738, L13

Nava, L., Sironi, L., Ghisellini, G., Celotti, A., & Ghirlanda, G. 2012, ArXiv e-prints

Ouyed, R., Staff, J., & Jaikumar, P. 2011, ApJ, 743, 116

Paczynski, B. & Xu, G. 1994, ApJ, 427, 708

Pe'er, A. 2012, ApJ, 752, L8

Pe'er, A. & Loeb, A. 2012, J. Cosmology Astropart. Phys., 3, 7

Pe'er, A. & Waxman, E. 2004, ApJ, 613, 448

Pe'er, A. & Wijers, R. A. M. J. 2006, ApJ, 643, 1036

Piran, T. 1999, Phys. Rep., 314, 575

Piran, T., Shemi, A., & Narayan, R. 1993, MNRAS, 263, 861

Quataert, E. & Kasen, D. 2012, MNRAS, 419, L1

Racusin, J. L., Karpov, S. V., Sokolowski, M., Granot, J., Wu, X. F., Pal'Shin, V., Covino, S., van der Horst, A. J., Oates, S. R., Schady, P., Smith, R. J., Cummings, J., Starling, R. L. C., Piotrowski, L. W., Zhang, B., Evans, P. A., Holland, S. T., Malek, K., Page, M. T., Vetere, L., Margutti, R., Guidorzi, C., Kamble, A. P., Curran, P. A., Beardmore, A., Kouveliotou, C., Mankiewicz, L., Melandri, A., O'Brien, P. T., Page, K. L., Piran, T., Tanvir, N. R., Wrochna, G., Aptekar, R. L., Barthelmy, S., Bartolini, C., Beskin, G. M., Bondar, S., Bremer, M., Campana, S., Castro-Tirado, A., Cucchiara, A., Cwiok, M., D'Avanzo, P., D'Elia, V., Della Valle, M., de Ugarte Postigo, A., Dominik, W., Falcone, A., Fiore, F., Fox, D. B., Frederiks, D. D., Fruchter, A. S., Fugazza, D., Garrett, M. A., Gehrels, N., Golenetskii, S., Gomboc, A., Gorosabel, J., Greco, G., Guarnieri, A., Immler, S., Jelinek, M., Kasprowicz, G., La Parola, V., Levan, A. J., Mangano, V., Mazets, E. P., Molinari, E., Moretti, A., Nawrocki, K., Oleynik, P. P., Osborne, J. P., Pagani, C., Pandey, S. B., Paragi, Z., Perri, M., Piccioni, A., Ramirez-Ruiz, E., Roming, P. W. A., Steele, I. A., Strom, R. G., Testa, V., Tosti, G., Ulanov, M. V., Wiersema, K., Wijers, R. A. M. J., Winters, J. M., Zarnecki, A. F., Zerbi, F., Mészáros, P., Chincarini, G., & Burrows, D. N. 2008, Nature, 455, 183

Rees, M. J. 1988, Nature, 333, 523

Rees, M. J. & Meszaros, P. 1992, MNRAS, 258, 41P

—. 1994, ApJ, 430, L93

Rybicki, G. B. & Lightman, A. P. 1979, Radiative processes in astrophysics

Sari, R. & Piran, T. 1995, ApJ, 455, L143

Sari, R., Piran, T., & Narayan, R. 1998, ApJ, 497, L17+

Siemiginowska, A., Stawarz, L., Cheung, C. C., Harris, D. E., Sikora, M., Aldcroft, T. L., & Bechtold, J. 2007, ApJ, 657, 145

Socrates, A. 2012, ApJ, 756, L1

Stone, N. & Loeb, A. 2012, Physical Review Letters, 108, 061302

Strubbe, L. E. & Quataert, E. 2009, MNRAS, 400, 2070

Ulmer, A. 1999, ApJ, 514, 180

van Paradijs, J., Kouveliotou, C., & Wijers, R. A. M. J. 2000, ARA&A, 38, 379

van Velzen, S., Körding, E., & Falcke, H. 2011, MNRAS, 417, L51

Wang, F. Y. & Cheng, K. S. 2012, MNRAS, 421, 908

Waxman, E. 1997, ApJ, 491, L19

Zauderer, B. A., Berger, E., Soderberg, A. M., Loeb, A., Narayan, R., Frail, D. A., Petitpas, G. R., Brunthaler, A., Chornock, R., Carpenter, J. M., Pooley, G. G., Mooley, K., Kulkarni, S. R., Margutti, R., Fox, D. B., Nakar, E., Patel, N. A., Volgenau, N. H., Culverhouse, T. L., Bietenholz, M. F., Rupen, M. P., Max-Moerbeck, W., Readhead, A. C. S., Richards, J., Shepherd, M., Storm, S., & Hull, C. L. H. 2011, Nature, 476, 425